RESEARCH ARTICLE

NANO · MICRO small
www.small-journal.com

Electrochemical Investigations of Sulfur-Decorated Organic Materials as Cathodes for Alkali Batteries

Qiang Fu, Lei Zhao, Xianlin Luo, Jan Hobich, Daniel Döpping, David Rehnlund, Hatice Mutlu, and Sonia Dsoke**

Alkali metal–sulfur batteries (particularly, lithium/sodium- sulfur (Li/Na–S)) have attracted much attention because of their high energy density, the natural abundance of sulfur, and environmental friendliness. However, Li/Na–S batteries still face big challenges, such as limited cycle life, poor conductivity, large volume changes, and the "shuttle effect" caused by the high solubility of Li/Na–polysulfides. Herein, novel organosulfur-containing materials, i.e., *bis*(4-hydroxy-2,2,6,6-tetramethylpiperidin-1-yl)disulfide (BiTEMPS-OH) and 2,4-thiophene/arene copolymer (TAC) are proposed as cathode materials for Li and Na batteries. BiTEMPS-OH shows an initial discharge/charge capacity of 353/192 mAh g^{-1} and a capacity of 62 mAh g^{-1} after 200 cycles at 100 mA g^{-1} in ether-based Li-ion electrolyte. Meanwhile, TAC has an initial discharge/charge capacity of 270/248 mAh g^{-1} and better cycling performance (106 mAh g^{-1} after 200 cycles) than BiTEMPS-OH in the same electrolyte. However, the rate capability of TAC is limited by the slow diffusion of Li-ions. Both materials show inferior electrochemical performances in Na battery cells compared to the Li analogs. X-ray powder diffraction reveals that BiTEMPS-OH loses its crystalline structure permanently upon cycling in Li battery cells. X-ray photoelectron spectroscopy demonstrates the cleavage and partially reversible formation of S—S bonds in BiTEMPS-OH and the formation/decomposition of thick solid electrolyte interphase on the electrode surface of TAC.

1. Introduction

Nowadays, humanity is facing challenges such as global warming and climate change due to excessive usage of fossil fuels (coal, oil, and gas) in the past decades. Therefore, it is of great urgency to generate energy in a sustainable manner.[1] In particular, renewable energy sources such as geothermal, biomass, wind, and solar, which are safe, abundant, and environmentally friendly, play essential roles in modern society and dramatically increase their shares.[2] Still, exploiting renewable energies is not an easy task due to its discontinuous supply and high dependence on climatic and geographic conditions. The development of energy storage systems that are directly or indirectly capable of storing clean energy will be a crucial issue to meet the demand of our society since people have a much tighter relationship with electricity than ever before.[2,3]

Lithium-ion batteries (LIBs) have dominated the market since their commercialization in 1991 because of their higher specific energy, energy density, and long

Q. Fu, L. Zhao, X. Luo, D. Rehnlund, S. Dsoke
Institute for Applied Materials (IAM)
Karlsruhe Institute of Technology (KIT)
Hermann-von-Helmholtz-Platz 1, D, 76344 Eggenstein-Leopoldshafen, Germany
E-mail: sonia.dsoke@kit.edu

J. Hobich, D. Döpping, H. Mutlu
Institute for Biological Interfaces 3 (IBG 3)
Karlsruhe Institute of Technology (KIT)
Hermann-von-Helmholtz-Platz 1, D, 76344, Germany, Eggenstein-Leopoldshafen
E-mail: hatice.mutlu@uha.fr

The ORCID identification number(s) for the author(s) of this article can be found under https://doi.org/10.1002/smll.202311800

DOI: 10.1002/smll.202311800

Q. Fu
Division of Energy Storage
Dalian Institute of Chemical Physics
Chinese Academy of Sciences
Dalian 116023, China

H. Mutlu
Institut de Science des Matériaux de Mulhouse
UMR 7361 CNRS/ Université de Haute Alsace
15 rue Jean Starcky, Mulhouse Cedex 68057, France

S. Dsoke
Fraunhofer Institute for Solar Energy Systems
Heidenhofstr. 2, 79110 Freiburg, Germany

S. Dsoke
Department of Sustainable Systems Engineering (INATECH)
University of Freiburg
79110 Freiburg, Germany

lifetime compared to other conventional batteries (lead-acid and nickel–cadmium batteries).[4] In addition, LIBs have a low self-discharge rate and no memory effect and they can be quickly charged due to their prominent cycling and rate performance.[5] Although LIBs are currently very popular on the market, they cannot meet the growing demand for large-scale energy storage due to the low lithium abundance, high cost, and potential safety concerns.[6]

Alternative systems have been developed in recent years, such as alkali metal–sulfur batteries (Li/Na–S), and metal–organic batteries.[7] Li/Na–S batteries based on a conversion reaction have attracted much attention because of their high energy density, natural abundance of elemental sulfur (S), and environmental friendliness. Conventional Na–S batteries based on solid electrolyte, molten Na, and molten sulfur operate in a temperature range of 300–350 °C.[8] The research for low-temperature or room-temperature Na–S batteries using a metallic Na anode, a sulfur cathode, and electrolytes based on organic solvents or polymers is currently in its infancy.[9] However, room temperature Li/Na–S batteries are challenged by several unsolved problems,[10] such as limited cycle life, poor conductivity, low density of elemental sulfur, large volume changes during cycling, and "shuttle effect" due to the high solubility of Li (Na) -polysulfides in common organic liquid electrolytes.[11] These polysulfides can diffuse to the Li (Na) anode and be reduced by the alkali metal (Li/Na), which causes rapid capacity loss, poor cycling stability, and low coulombic efficiency. Many efforts have been made to solve the above-mentioned problems, such as the use of sulfur composites, where elemental sulfur is often confined in mesoporous/microporous hosts to form composites.[12]

A metal–organic battery consists of a metallic anode and an organic cathode in a carbonate- and/or ether-based electrolyte, and the cathode material can be divided into P-type, N-type, and B-type materials based on their redox mechanisms (depending on the properties of donating (P-type), accepting electrons (N-type), and bi-functional (B-type), respectively).[13] Organic materials have been intensively studied for several decades and have become rational alternatives for cathode materials due to their abundant resources, high theoretical capacity, environmental friendliness, and structure design. For instance, the prototype concept of organic cathode materials can be traced back to the early 1970s, when an organic compound $(CF_x)_n$–Li was first applied as cathode material in commercial primary lithium batteries.[14] The conjugated polymers, including polythiophene and polyparaphenylene, have already been used as cathode materials in batteries and have been intensively studied over the past decades.[15] Their electrochemical performance has been greatly improved by tuning the electrolyte systems,[16] modifying polymer structures,[17] and introducing additives.[18] Among these methods, designing new polymer structures is the most attractive choice because the properties of polymers can be properly altered to achieve better electrochemical performances. While the electrochemical performance of conjugated polymers based on a single monomer is reported in many publications, the use of 2,4-thiophene/arene copolymer (TAC) has not been reported.

Organosulfur-containing materials are promising cathodes for advanced batteries because of their low cost, sustainability, high theoretical capacity, and environmental friendliness.[19] However, they still face some intrinsic problems such as low conductivity, high solubility in electrolytes, and poor stability.[19] Indeed, the redox-active sulfur in organosulfur materials strongly bonded with carbon or other heteroatoms can effectively alleviate the shuttle effect.[19a,20] The electronic conductivity of organosulfur materials can be improved through Se-doping,[21] combination with multi-walled carbon nanotube,[22] and highly crosslinking structures with the thiourea aldehyde resin backbones.[23] In this regard, *bis*(2,2,6,6-Tetramethylpiperidine-1-sulfanyl) (BiTEMPS) derivatives and TAC are promising candidates for cathode materials in Li and Na batteries since they can be designed and synthesized by combining the advantages of both organic materials and the element sulfur. The synthesis of BiTEMPS was initially reported by Bennett et al. in 1967,[24] in which an unfunctionalized BiTEMPS disulfide (BiTEMPS-2S) was first synthesized by reacting piperidine precursor with sulfur dichloride in N,N-dimethylformamide (DMF).[25] *Bis*(4-hydroxy-2,2,6,6-tetramethylpiperidin-1-yl)disulfide (BiTEMPS-OH) as a BiTEMPS derivative was first designed by Otsuka's group in 2017.[26] The S—S bond dissociation energy (BDE) of BiTEMPS-OH was estimated to be ≈110 kJ mol^{-1}, which is also close to that of unfunctionalized BiTEMPS-2S calculated by Maillard. Furthermore, BiTEMPS-OH also shows good stability at 100 °C in air, suggesting that the dissociation reaction of S—S bond can be utilized without special care under atmospheric conditions. BiTEMPS-OH, as one of BiTEMPS derivatives, is expected to be a promising candidate for organic cathode materials because it has good air stability and a special functional structure *N—S—S—N* with a low BDE of the S—S bond in the molecule. However, the electrochemical performance of BiTEMPS-OH has not been reported yet. Therefore, this material, BiTEMPS-OH, is expected to be promising as cathode material in Li and Na batteries.

Herein, we propose novel organosulfur-containing materials, including BiTEMPS-OH and TAC, as cathodes for Li and Na batteries. Their electrochemical performances are evaluated in ether-based electrolytes. Meanwhile, their redox mechanisms and kinetics are studied by using ex situ X-ray powder diffraction (XRD) and X-ray photoelectron spectroscopy (XPS) techniques, as well as electrochemical impedance spectroscopy (EIS).

2. Experimental Section

2.1. Materials Synthesis

Organic materials, BiTEMPS-OH and thiophene/arene copolymer (TAC), as shown in **Figure 1**, were synthesized using the same methods previously reported by Mutlu and colleagues[27] (The detailed methods are listed in the Supporting information). The respective chemical structural characterization performed via nuclear magnetic resonance (NMR) was in line with the reported data, demonstrating that both synthesized materials were pure (Figure S1–S6, Supporting information). The repeating unit of TAC consists of one 2,4-substituted thiophene and one *para*-substituted phenylene. In addition, the copolymer also contains a C = S structure in its end group. It had number average molecular weight (M_n) and weight average molecular weight (M_w) of 1360 and 2430 g mol^{-1}, respectively. BiTEMPS-OH was light yellow (Figure S7, Supporting information), while TAC has an orange–brown appearance because of its conjugated structure and corresponding light absorption properties. Note that

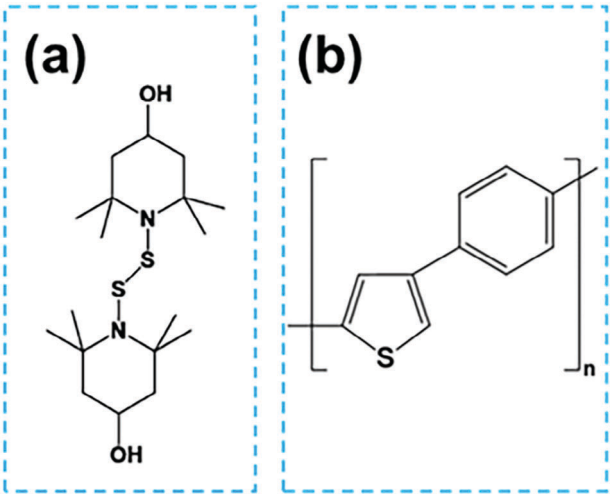

Figure 1. Structures of *Bis*(4-hydroxy-2,2,6,6-tetramethylpiperidin-1-yl)disulfide (BiTEMPS-OH) a) and thiophene/arene copolymer (TAC) b), respectively.

theoretical capacities for BiTEMPS-OH and TAC based on two-electron reactions were 143 and 335 mAh g^{-1}, respectively.

2.2. Structural Characterization

XRD was performed using a STOE STADI P diffractometer with (Mo $K_{\alpha 1}$ radiation, λ = 0.70932 Å, 50 kV, 40 mA) in Debye-Scherrer geometry equipped with Mythen1K detectors. The 2θ scan range was set from 1° to 50° with a step size of 0.015°. The powder diffraction patterns were measured in capillary geometry with powders filled in 0.5 mm Ø boro–silicate capillaries. XPS was performed using a K-Alpha spectrometer (ThermoFisher Scientific, UK) equipped with a micro-focused, monochromated Al Kα X-ray source (λ = 1486.6 eV) with a spot size of 400 µm. All samples were prepared in an argon-filled glovebox and transferred under an inert atmosphere into the spectrometer. All spectra were referenced to the carbonaceous C 1s peak (C–C/C–H) at 285.0 eV binding energy.

2.3. Electrolyte Preparation

The preparation of electrolytes was carried out in a glovebox (MBraun) under an Ar atmosphere with very low H_2O and O_2 content (<0.5 ppm). LiTFSI, DME, DOL, $NaCF_3SO_3$, and TEGDME refer to lithium *bis*(trifluoromethanesulfonyl)imide (Sigma Aldrich, 99.95%), 1,2-dimethoxyethane (Sigma Aldrich, 99.5%), 1,3-dioxolane (Sigma Aldrich, 99.8%), sodium trifluoromethanesulfonate (Tokyo Chemical Industry, >98%), and tetraethylene glycol dimethyl ether (Sigma Aldrich, >99%), respectively. Both Li/Na-based electrolytes, including 1 M LiTFSI in DME-DOL (v/v = 1:1) and 1 M $NaCF_3SO_3$ in TEGDME, were prepared by dissolving corresponding salts into solvents with vigorous stirring overnight at room temperature in the glovebox. All the salts were first dried in a vacuum dryer at 120 °C for 48 h. TEGDME was dried with 4 Å molecular sieves inside the glovebox for 48 h.

2.4. Electrochemical Characterization

The slurry mixture consists of 60wt.% of the active material, 30wt.% of C65, and 10wt.% of polyvinylidene difluoride (PVDF) dissolved in *N*-methyl-2-pyrrolidone. Organic cathodes were prepared by coating a slurry mixture on aluminum foil with a wet thickness of 110 µm. The coated electrode was dried at 60 °C for 24 h and then punched into disks of 12 mm diameter (active materials mass loading: 0.5–1.0 mg cm^{-2}). The disks were then vacuum-dried at 60 °C for 24 before being transferred into the glovebox. The electrochemical performance was studied at 25 °C in 2032-type coin cells using Li or Na metal as the negative and the above-mentioned disks as the positive electrode with Whatman separator and 60 µL 1 M LiTFSI in DME/DOL (v/v = 1:1) or 1 M $NaCF_3SO_3$ in TEGDME as an electrolyte in a glovebox. The galvanostatic cycling tests were performed on a VMP-3 potentiostat (BioLogic Science Instruments). Li-based cells were cycled at current densities of 100 mA g^{-1} in the voltage ranges of 0.5–3.0 V and 0.8–3.0 V versus Li^+/Li for BiTEMPS-OH and TAC, respectively. Na-based cells were cycled at a current density of 100 mA g^{-1} and in different voltage ranges (0.5 V-2.7 V, 0.2-2.7 V, and 0.2-3.0 V versus Na^+/Na) for BiTEMPS-OH and (0.8 V-2.7 V, 0.5-3.0 V and 0.2-3.0 V versus Na^+/Na) for TAC, respectively. The rate performance of BiTEMPS-OH and TAC were carried out in Li-based cells in the voltage ranges of 0.5-3.0 V versus Li^+/Li and 0.8-3.0 V versus Li^+/Li for TAC, respectively. Cyclic voltammetry measurements were carried out at different scan rates with the voltage ranges of 0.5-3.0 V versus Li^+/Li for BiTEMPS-OH and 0.8-3.0 V versus Li^+/Li for TAC in Li cells. In Na systems, the voltage ranges are 0.2-2.7 V versus Na^+/Na for BiTEMPS-OH and 0.5-3.0 V versus Na^+/Na for TAC. Both BiTEMPS-OH and TAC cathode disks were immersed for 24 h in the LiTFSI-DME/DOL electrolyte to examine the solubility of materials (Figure S8, Supporting information). Compared with the blank one, it shows no notable color change for the BiTEMPS-OH one, while–yellow color for the TAC can be clearly seen, suggesting that TAC is somehow soluble in the ether-based electrolyte. Unfortunately, this is unexpected for the TAC. Note that only a limited amount of electrolyte (60 µL) was used in the cells, one can expect that a limited amount of active TAC material was dissolved during the cycling.

Electrochemical impedance spectroscopy (EIS) measurements were performed for the Li-based cells with BiTEMPS-OH and TAC cathodes. The electrochemical impedance spectra were recorded with an amplitude of 5 mV over the frequency range from 1 to 10 mHz. For ex situ XRD and XPS, the cells were disassembled after cycling and the electrodes were washed with a mixture of DME/DOL (v/v = 1:1) three times and dried in a vacuum chamber for 24 h at room temperature in an Ar-filled glovebox.

3. Results and Discussion

3.1. Electrochemical Performance in Li-Based Cells

LiTFSI-based electrolyte is selected to study the performance of the sulfur–organic electrodes since 1 M LiTFSI in a mixture of DME and DOL (v/v = 1:1) is an ether-based electrolyte widely used in Li–S batteries.[28]

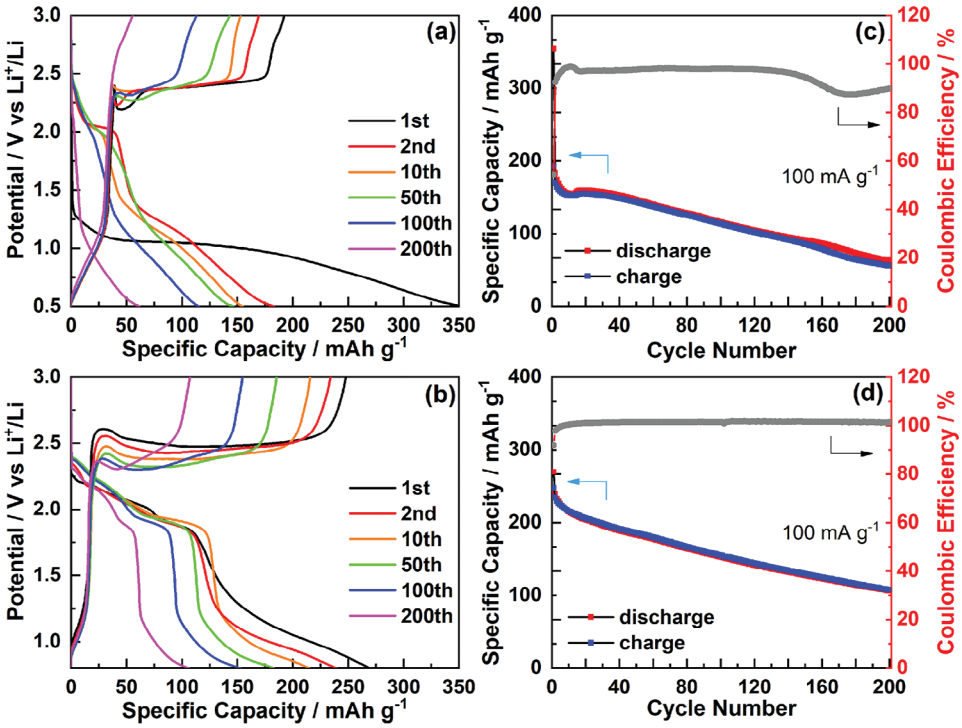

Figure 2. Discharge–charge profiles and cycling performance of BiTEMPS-OH a,c) and TAC b,d) at 100 mA g^{-1} in 1 M LiTFSI in DME-DOL (v/v = 1:1) using coin cells.

Figure 2 displays the discharge–charge profiles and cycling performance of both BiTEMPS-OH and TAC at 100 mA g^{-1}. Note that the specific current density of 100 mA g^{-1} corresponds to the value of 0.1 mA cm^{-2} when considering active materials mass loading of 1.0 mg cm^{-2}. As shown in Figure 2a (Figure S9a, Supporting information), BiTEMPS-OH exhibits a long plateau at 1.1 V, followed by a long slope for the first discharge, one short plateau at 2.2 V, and a long plateau at 2.4 V for the first charge. In the second cycle, BiTEMPS-OH displays two discharge plateaus at ≈2.0 and 1.3 V and a charge plateau at ≈2.4 V. All the plateaus become shorter during cycling and completely disappear after 200 cycles. In contrast, TAC shows a different behavior during cycling as displayed in Figure 2b (Figure S9b, Supporting information). TAC demonstrates two plateaus at 2.1 and 1.9 V for the initial discharge and a long plateau at 2.5 V for the initial charge. In the following cycle, TAC has two discharge plateaus at 2.1 and 1.9 V, followed by a long slope and charge plateau at ≈2.4 V. TAC displays shorter discharge/charge plateaus and a decrease of the charge potential plateau after 200 cycles. This suggests that most of BiTEMPS-OH becomes electrochemically inactive after prolonged cycling while part of TAC is still active, which may be related to the dissolution of organic materials during cycling. In contrast, elemental sulfur shows two slightly higher discharge plateaus and a slope profile, which is attributed to the reduction of cyclo-S_8 molecule to longer-chain polysulfides (Li_2S_n, $4 \leq n \leq 8$, 2.3 V) and the formation of short-chain sulfides (Li_2S_2, 2.1 V) and Li_2S, respectively.[29] BiTEMPS-OH delivers an initial discharge/charge capacity of 353/192 mAh g^{-1}, leading to an initial CE of 54% and discharge capacity of 62 mAh g^{-1} after 200 cycles with capacity retention of 34% (compared to second discharge capacity of 183 mAh g^{-1}) (Figure 2c). Note that the initial discharge of BiTEMPS-OH is much higher than its theoretical capacity of 143 mAh g^{-1} and this extra capacity can be mainly attributed to the SEI formation during cycling since the possible side reactions between the organosulfur species and the electrolyte cannot be completely excluded.

Meanwhile, TAC exhibits an initial discharge/charge capacity of 270/248 mAh g^{-1} with a much higher initial CE of 92% (Figure 2d). TAC shows a higher discharge capacity of 106 mAh g^{-1} after 200 cycles with a higher capacity retention of 44% (compared to the second discharge capacity of 239 mAh g^{-1}). The CE of BiTEMPS-OH slowly increases to 98–99% after 15 cycles, and it drops to 88% after 150 cycles and then slightly increases to 90%. The CE fluctuation may be attributed to the disappearance of the plateaus after 150 cycles, resulting in a distinct reduction of the charge capacity. On the contrary, the CE of TAC first increases from 91% to 99% at the very beginning and stabilizes ≈100%–101% during the following 200 cycles, implying that TAC has a much better electrochemical performance in the LiTFSI-DME/DOL electrolyte. Note that the loss of S-species from both organic materials may be responsible for the inferior CE during cycling, which is often observed in the Li–S batteries.[29] Moreover, despite their low capacity retention along cycling, both materials show higher initial capacities compared with other materials reported in the literature (shown in Table S1, Supporting information), implying that they are promising cathode materials. Of course, further work such as electrode engineering with conductive carbon materials should be done to improve the electrochemical performance by restraining the dissolution of organic materials.

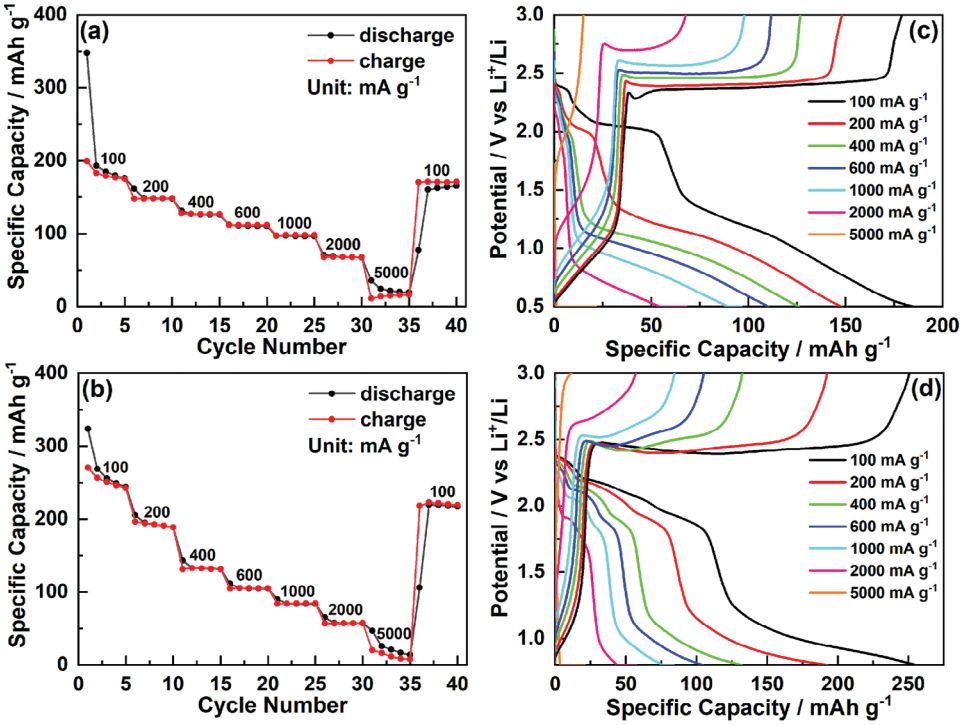

Figure 3. Rate performance and discharge–charge profiles of BiTEMPS-OH a,c) and TAC b,d) at different current densities in 1 M LiTFSI in DME-DOL (v/v = 1:1) using coin cells.

Rate capability tests were performed to evaluate the electrochemical performances of BiTEMPS-OH and TAC at different current densities, as shown in **Figure 3**. The capacity of BiTEMPS-OH reaches 180, 148, 126, 110, 96, and 68 mAh g^{-1} at 100, 200, 400, 600, 1000, and 2000 mA g^{-1}, respectively (Figure 3a, corresponding values of 0.1, 0.2, 0.4, 0.6, 1.0, and 2.0 mA cm^{-2} with mass loading of 1.0 mg cm^{-2}). Then, the capacity drops drastically to 21 mAh g^{-1} at a high current density of 5000 mA g^{-1}. When the current density returns to 100 mA g^{-1}, the specific capacity recovers to 163 mAh g^{-1}. Meanwhile, TAC shows specific capacities of 250, 192, 132, 105, 84, and 57 mAh g^{-1} at 100, 200, 400, 600, 1000, and 2000 mA g^{-1}, respectively, and only maintains 19 mAh g^{-1} at 5000 mA g^{-1}. When the current density returns to 100 mA g^{-1}, TAC still displays a specific capacity of 219 mA g^{-1} with a capacity retention of 88% (Figure 3b). Both materials demonstrate the increase of charge potentials and decrease of discharge potentials along with the increase of current densities because of higher polarization at higher current densities (Figure 3c,d; Figure S10a,b, Supporting information). To sum up, TAC shows higher capacities than BiTEMPS-OH when the current density is lower than 400 mA g^{-1}, while TAC shows a relatively worse rate performance than BiTEMPS-OH, especially at very higher current densities. This phenomenon can be attributed to the slow diffusion process of Li-ions in and out of the polymer backbone.[15] When a high current density is applied, it can be inferred that the electrochemical reaction takes place mostly on the surface of the TAC cathode and the inner regions of the conjugated polymer are probably not involved, leading to lower material utilization and capacity loss.

3.2. Electrochemical Performance in Na-Based Cells

To study the electrochemical performance of BiTEMPS-OH and TAC in Na-based cells, 1 M $NaCF_3SO_3$ in TEGDME electrolyte was selected since it has already been used for both Na-ion and Na–S batteries.[30] Figure S11, (Supporting information) displays charge–discharge curves and cycling performance of BiTEMPS-OH and TAC in the voltage range of 0.5–2.7 V and 0.8–2.7 V at 100 mA g^{-1}, respectively. For the initial cycle, BiTEMPS-OH has a long discharge plateau at 0.8 V and two charge plateaus at ≈2.0 and 2.3 V, and the discharge plateau disappears in the following two cycles. In contrast, TAC only shows sloping discharge curves in the $NaCF_3SO_3$-TEGDME electrolyte. A short charge plateau can be found at ≈1.8 V in the initial charge curve and almost disappears after the third cycle.

BiTEMPS-OH and TAC deliver an initial discharge capacity of 190 and 128 mA g^{-1} during the first cycle (Figure S11, Supporting information), respectively. However, the capacity for both materials decays very fast during the initial ten cycles and stabilizes to a capacity of 22 mAh g^{-1} after 200 cycles and it still fades quickly along cycling even in different voltage ranges (Figure S12, Supporting information). Compared with those for Li cells, it seems that both materials in Na cells do not show promising electrochemical performance. This may suggest that most of the active material fails to participate in the reversible redox reaction, probably due to the irreversible reaction of BiTEMPS radicals with the electrolyte during the initial cycle.[31] However, the underlying mechanism behind this needs to be investigated in future studies.

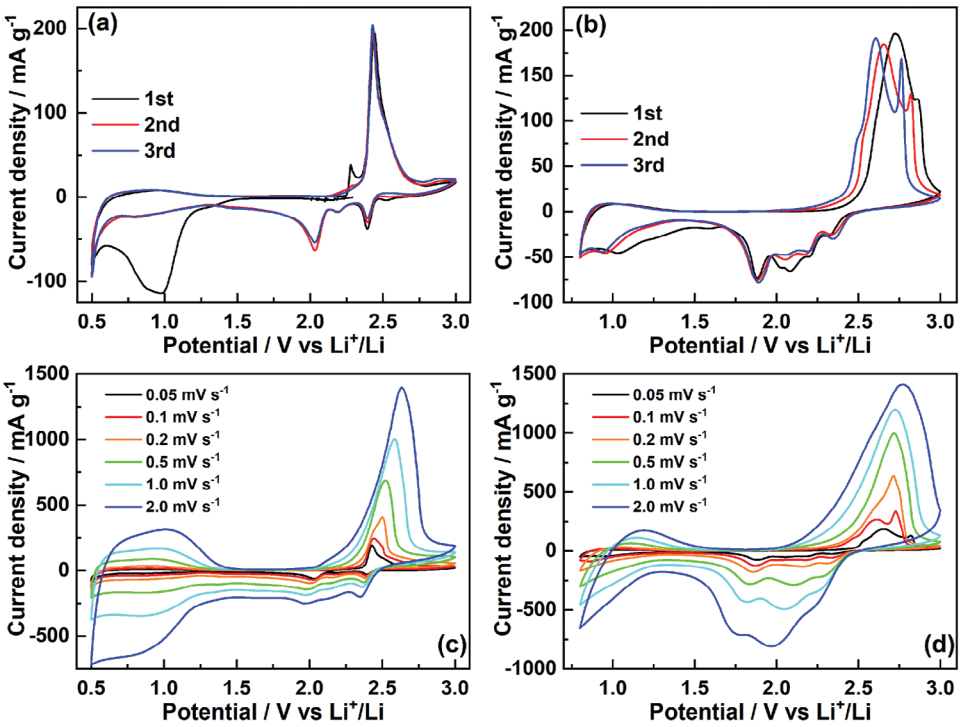

Figure 4. CV curves of BiTEMPS-OH a,c) and TAC b,d) at 0.05 mV s^{-1} and at different scan rates in 1 M LiTFSI in DME-DOL (v/v = 1:1) using coin cells.

3.3. Reaction Mechanism in Li-Based Cells

To have a better understanding of the reaction mechanism, multiple analytical techniques are used, including cyclic voltammetry (CV), XRD, and XPS. CV was carried out on electrodes in the voltage range of 0.5–3.0 V at a scan rate of 0.05 mV s^{-1}, as shown in **Figure** 4a,b. For BiTEMPS-OH, a broad reduction peak at 0.97 V can be observed in the initial scan, consistent with an initial discharge curve of BiTEMPS-OH that is attributed to the redox reaction of active material and SEI formation during the initial discharge process. In the initial oxidative scan, a small oxidation peak at 2.28 V and a main sharp oxidation peak at 2.44 V appear. In the following two scans, three reversible reduction peaks appear at 2.39, 2.19, and 2.03 V, respectively. The main oxidation peak with a high current at 2.43 V remains stable while the small peak at 2.28 V disappears, which may be attributed to the activation process of the material (e.g., high energy barrier) during the first charge process. All the reversible oxidation and reduction peaks are well-matched with their discharge and charge plateaus in the galvanostatic cycling tests. Meanwhile, the second and third CV curves are almost overlapping (with only minor intensities decrease of the reduction peaks), indicating high electrochemical reversibility of the redox reactions. The results suggest that BiTEMPS-OH undergoes a three-step reduction process and can be oxidized in one step. Nevertheless, elemental sulfur exhibits two typical reduction peaks at 2.3 and 1.9 V and an oxidation peak at 2.4–2.5 V, corresponding to the reduction of elemental sulfur (S_8) to long-chain lithium polysulfides (Li_2S_x) ($4 < x < 8$) and the formation of short-chain Li_2S_2/Li_2S, and phase transformation to elemental sulfur, respectively.[29a,32]

For TAC (OCV, 2.49 V), four reduction peaks emerge at 1.03, 1.88, 2.08, and 2.31 V, and one oxidation peak appears at 2.72 V with a small shoulder at 2.86 V. During the following scans, minor changes for reduction peaks with slightly lower intensities can be observed, while the oxidation peak shifts to 2.65 and 2.61 V, respectively, and the shoulder grows up with shifts to 2.82 V and 2.76 V. According to the CV results, TAC has broad oxidation and reduction peaks, attributed to a typical feature of conductive polymers.[33] Based on the general redox mechanism of conjugated polymers, the oxidation and reduction peaks are attributed to the redox reaction of TAC and the corresponding incorporation/release of Li-ions in and out of flexible host polymer matrixes.[34]

To further study the kinetics of the redox reaction, CV was performed at different scan rates, as shown in Figure 4c,d. For both materials, the anodic and cathodic peaks tend to shift to lower and higher potential as the scan rate increases, respectively. Generally, peak current (i) and scan rate (v) obey the power-law relationship as:[35] $i = av^b$. Typically, the b value of 0.5 represents a diffusion-controlled process and the value of 1.0 suggests a surface-controlled process. Figure S13 (Supporting information) shows the linear fitting result of the oxidation and reduction peaks of BiTEMPS-OH and TAC. For BiTEMPS-OH and TAC, the b value of most peaks is less than 0.6 and close to 0.5, indicating diffusion-controlled processes. While only the reduction peak at 2.05 for TAC has the b value of 0.76, indicating the mix-controlled process.

Ex situ XRD was performed to study the crystallinity and structural evolution of BiTEMPS-OH during the initial charge–discharge processes. **Figure** 5a shows a series of sharp reflections, indicating the crystalline features of BiTEMPS-OH. For

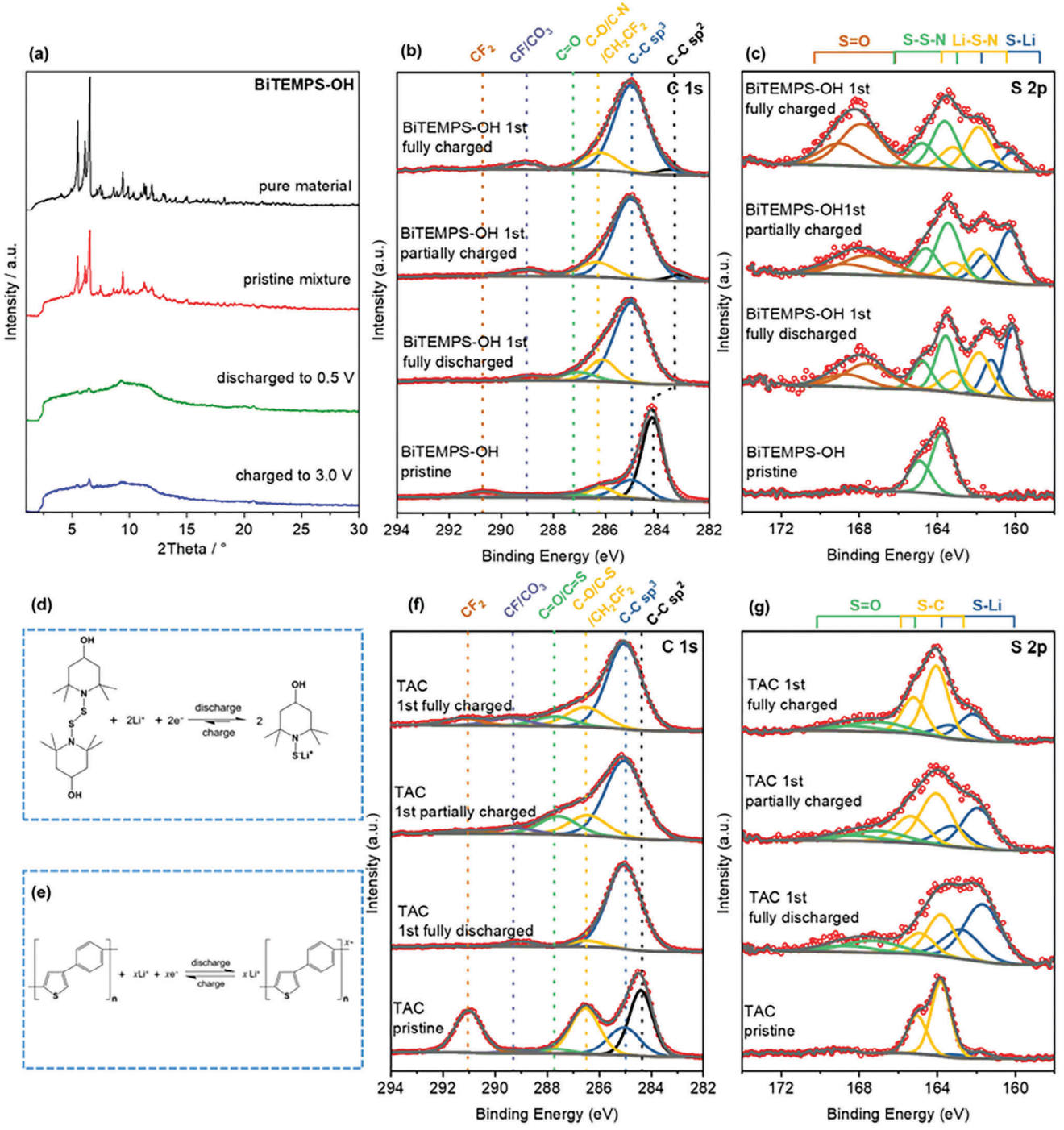

Figure 5. Ex situ XRD of BiTEMPS-OH a), C 1s and S 2p spectra of BiTEMPS-OH b,c) and TAC f,g) at different charged and discharged states, and proposed redox mechanism of BiTEMPS-OH d) and TAC e) in Li cells, respectively.

BiTEMPS-OH, the pristine electrode mixture shows similar reflections to that of the pure material in terms of positions of diffraction peaks, with slightly decreased intensities, indicating that no chemical transformation occurs and the crystallinity of BiTEMPS-OH does not decrease much during the cathode preparation. These sharp reflections disappear and only a few small broad reflections exist for the discharged BiTEMPS-OH at 0.5 V, indicating the significant changes in the crystal structure to an amorphous phase after the reduction process. After BiTEMPS-OH is charged to 3 V, the reflection at 6.5°, which is the peak with the highest intensity in the diffractograms of the pure material and pristine mixture, is slightly recovered. The comparison of XRD shows an irreversible transformation of BiTEMPS-OH from the crystalline to the amorphous state during cycling. The

possible reasons could be related to the damage of the polymer backbone, loss of S-species causing the backbone to break apart, or the incomplete transformation to initial BiTEMPS-OH.

To further investigate the redox mechanism of BiTEMPS-OH and TAC, ex situ XPS was performed on electrodes at different states, as displayed in Figure 5b,c,f,g, including the pristine and cycled cathodes, the first full discharged (discharged to 0.5 V for BiTEMPS-OH and to 0.8 V for TAC), the first partial charged (charged to 2.2 V for BiTEMPS-OH and to 2.4 V for TAC) and the first full (re)charged (charged to 3.0 V) ones.

For the pristine BiTEMPS-OH cathode, the C 1s spectrum (Figure 5b) is fitted by six peaks with binding energies at 284.2, 285.0, 286.2, 287.3, 289.0, and 290.7 eV, which are ascribed to sp^2 bonded carbon, sp^3-bonded carbon, C—O/C—N/CH_2CF_2, C = O, CF/CO_3, and CF_2, respectively.[36] The peaks of sp^2-bonded carbon and CF_2 can be attributed to the conductive carbon black and PVDF binder in the pristine cathode, respectively.[36c,d] In contrast to the pristine cathode, these two peaks cannot be observed in the spectrum of the cathode after the first fully discharged process, whose disappearance can be attributed to the formation of an SEI layer on the cathode surface. The signal of sp^2-bonded carbon is detected again after the first partial charge and the first full charge, indicating that the thickness of the SEI layer decreases during the charging process. For the pristine BiTEMPS-OH cathode (Figure 5c), the S 2p spectrum only shows one doublet with S $2p_{3/2}$ at 163.7 eV, assigned to *N—S—S—N*, which is lower than that of elemental sulfur (164.0 eV).[37] After the first discharging, the spectrum shows four doublets with binding energies of S $2p_{3/2}$ at 160.1, 161.8, 163.5, and 167.5 eV, respectively. This result confirms the cleavage of the S—S bonds in BiTEMPS-OH during the discharge process. Among these peaks, the doublet at a binding energy of 161.8 eV can be assigned to the Li–S–N structure, implying that the reduced species of BiTEMPS-OH can combine with Li-ions from the electrolyte. However, it is believed that only a part of the S—S bonds participates in the electrochemical reaction because the doublet with a binding energy of S $2p_{3/2}$ at 163.5 eV, which corresponds to *N—S—S—N*, is still present in the spectrum. The doublets at low binding energy (S $2p_{3/2}$ at 160.1 eV) and high binding energy (S $2p_{3/2}$ at 167.9 eV) are attributed to lithium sulfide and S = O from LiTFSI, respectively.[38] Compared with the spectrum of the sample after the first full discharge, the relevant peaks can still be observed at the partial and full charging states. The intensity of the *N—S—S—N* peak increases, but this phenomenon is not obvious, indicating that the S—S bonds can only be partially reformed during the charging process. Based on the result of ex situ XPS, it is confirmed that the S—S bond in BiTEMPS-OH can partially break and reform during cycling, and therefore the proposed redox mechanism is described in Figure 5d.

For the pristine TAC cathode, the C 1s spectrum (Figure 5f) is fitted by six peaks with binding energies at 284.4, 285.0, 286.5, 287.7, 289.2, and 291.0 eV, which are assigned to sp^2 bonded carbon, sp^3 bonded carbon, C—O/C—S/CH_2CF_2, C = O/C = S, CF/CO_3 and CF_2, respectively.[36] Among these peaks, the C = S peak with low intensity is attributed to the end group of the copolymer. The peak of sp^2-bonded carbon and CF_2 can be attributed to the conductive carbon black and PVDF binder in the pristine cathode, respectively. In contrast to the pristine cathode, these two peaks disappear after the first full discharge. This result shows that a thick SEI layer is formed on the cathode surface during the discharge process, which blocks the signals of the conductive additive and binder in the cathode. The peak of CF_2 emerges in the spectrum of the first partially charged sample again and the peak intensity continues to increase as the cathode is charged to 3.0 V. This result suggests that the thickness of SEI layers gradually decreases during the charging process. The formation and decomposition of the SEI layer on the cathode surface can also be confirmed by the S 2p spectra, as presented in Figure 5g. For the pristine cathode, the spectrum shows two doublets. The doublet at a low binding energy of 161.8 eV (S $2p_{3/2}$) corresponds to C = S, which originates from the end group of the copolymer. The dominating doublet at 163.8 eV (S $2p_{3/2}$) is assigned to S—C, corresponding to the thiophene structure in TAC. After the first full discharge, the spectrum shows three doublets with binding energies at 161.6, 163.8, and 167.3 eV, respectively. The doublets at 163.8 eV (S $2p_{3/2}$) and 167.3 eV (S $2p_{3/2}$) are attributed to N—S and S = O from LiTFSI, respectively. The doublet at a low binding energy of 161.6 eV can be assigned to S = C or the Li—S bond between the thiophenes and Li-ions. Compared with the spectrum of the first full discharged sample, the intensity of the doublet at 163.9 eV (S $2p_{3/2}$) increases significantly during the charging process. This is because the S—C doublet of the copolymer becomes detectable again and overlaps with the N—S signal from LiTFSI. Therefore, the reduction of the SEI layer thickness can also be confirmed. As for the Li—S doublet, the peak intensity decreases during the charging process. This result may indicate that the interaction between TAC and Li-ions is weakening, and the Li-ions diffuse out of the polymer matrixes until the battery is fully charged. Based on the general redox mechanisms of conductive polymers, it is believed that TAC undergoes the N-type reaction (Figure 5e) in Li batteries because the upper limit of charging voltage is set up to 3 V, which is too low to initiate the P-type reaction. Meanwhile, it is impossible to activate the P-type reaction of TAC in the lithium battery because the corrosion of the aluminum current collector starts to take place in the LiTFSI-based electrolyte above ≈3.5–4.0 V versus Li^+/Li.[39] However, it should be mentioned that the signal variation of the Li—S doublet can also be attributed to the thickness reduction of the SEI layer on the cathode surface.

Electrochemical impedance spectroscopy (EIS) was further applied to investigate the electrochemical kinetic properties of both BiTEMPS-OH and TAC electrodes (**Figure 6**). In the case of OCV and fully charged samples (3.0 V), each Nyquist plot is composed of a semicircle in the high to the medium-frequency region and a sloped line in the low-frequency region, which corresponds to the charge transfer process (R_{ct}) and Li^+ ion diffusion in the electrode bulk (Warburg impedance, W), respectively. In contrast, two semicircles are observed for the fully discharged BiTEMPS-OH (0.5 V) and TAC (0.8 V), where the first semicircle is ascribed to the SEI film (R_f) and the second semicircle is attributed to the charge transfer process. The intercept on the *z'* axis at high frequency represents the internal resistance of the battery R_s. At OCV, BiTEMPS-OH shows a much higher internal resistance than TAC. At the fully discharged states, the formation of SEI film is also proven and agrees with XPS results above and the R_f for BiTEMPS-OH is much smaller than that of TAC, suggesting the faster kinetics of BiTEMPS-OH. Meanwhile, the presence of a single semicircle for both materials at 3.0 V indicates the

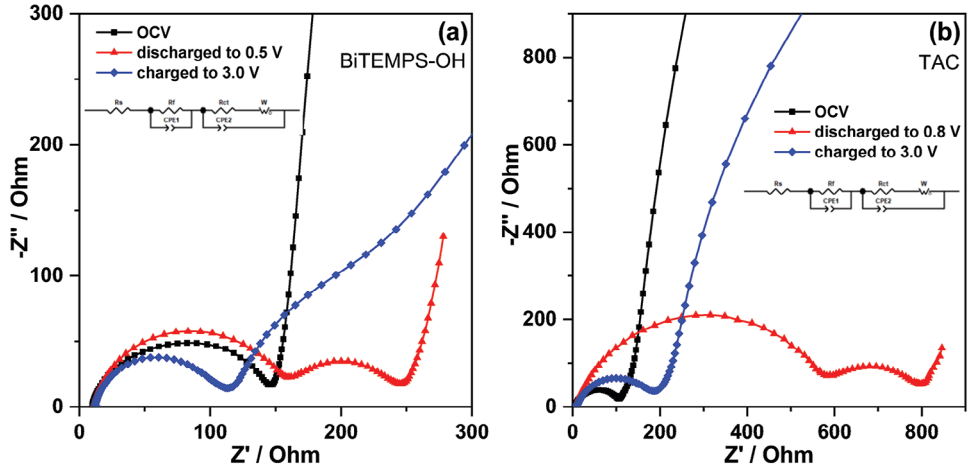

Figure 6. Nyquist plots of BiTEMPS-OH a) and TAC b) at OCV, fully discharged and fully charged states (Inset is the equivalent circuit used for the fully discharged state) in 1 M LiTFSI in DME-DOL (v/v = 1:1) using coin cells.

decomposition of SEI during the charging process, in accordance with XPS results.

4. Conclusion

This work presents BiTEMPS-OH and TAC applied, for the first time, as cathode materials in Li- and Na-based batteries. Their electrochemical performances and the redox mechanisms have been comprehensively studied by using different techniques. TAC exhibits much higher capacity and better cycling performance in Li battery cells than BiTEMPS-OH. However, the rate performance of TAC is inferior to BiTEMPS-OH and confined by the slow diffusion of Li-ions in the active material. Meanwhile, both BiTEMPS-OH and TAC materials demonstrate much poorer electrochemical performances in Na cells than in Li cells, suggesting that neither material is promising in Na cells. It is suspected that the high reactivity of metallic Na can be one of the reasons for this unsatisfying electrochemical performance since the Na anodes without protection can react with the electrolyte directly, even without electrochemical cycling tests. Therefore, metallic Na should be more carefully and effectively protected. In addition, ex situ XRD reveals that BiTEMPS-OH loses its crystalline structure permanently as they are cycled in Li cells. Ex situ XPS demonstrates the cleavage and partially reversible reformation of the S—S bond in BiTEMPS-OH during cycling because of the low BDE of the S—S bond and the formation/decomposition of SEI on the surface of the TAC electrode. Further work should be done to improve the electrochemical performance, which can be achieved via electrode engineering with conductive carbon materials to restrain the dissolution of organic materials.

Supporting Information

Supporting Information is available from the Wiley Online Library or from the author.

Acknowledgements

This work contributes to the research performed at CELEST (Center for Electrochemical Energy Storage Ulm-Karlsruhe) and was funded by the German Research Foundation (DFG) under Project ID 390874152 (POLiS Cluster of Excellence). H. M. acknowledges the University of Haute-Alsace for the financial support from the French National Research Agency with the reference "ANR-22-CPJ1-0077-01" and from the CNRS for the junior professorship contract.

Open access funding enabled and organized by Projekt DEAL.

Conflict of Interest

The authors declare no conflict of interest.

Data Availability Statement

The data that support the findings of this study are openly available in KITOpen at https://doi.org/10.35097/1756, reference number 1756.

Keywords

alkali batteries, BiTEMPS-OH, cathodes, organic materials, thiophene/arene copolymer

Received: December 18, 2023
Published online:

[1] X. Yu, A. Manthiram, *Adv. Energy Sustain. Res.* **2021**, *2*, 2000102.
[2] B. Dunn, H. Kamath, J.-M. Tarascon, *Science* **2011**, *334*, 928.
[3] Z. Yang, J. Zhang, M. C. W. Kintner-Meyer, X. Lu, D. Choi, J. P. Lemmon, J. Liu, *Chem. Rev.* **2011**, *111*, 3577.
[4] T. Kim, W. Song, D.-Y. Son, L. K. Ono, Y. Qi, *J. Mater. Chem. A* **2019**, *7*, 2942.
[5] G. Jeong, Y.-U. Kim, H. Kim, Y.-J. Kim, H.-J. Sohn, *Energy Environ. Sci.* **2011**, *4*, 1986.
[6] a) N. Zhang, X. Chen, M. Yu, Z. Niu, F. Cheng, J. Chen, *Chem. Soc. Rev.* **2020**, *49*, 4203; b) J.-Y. Hwang, S.-T. Myung, Y.-K. Sun, *Chem. Soc. Rev.* **2017**, *46*, 3529.
[7] a) D. Meggiolaro, M. Agostini, S. Brutti, *ACS Energy Lett.* **2023**, *8*, 1300; b) H. Ye, Y. Li, *Energy Fuels* **2021**, *35*, 7624.

[8] a) Z. Wen, J. Cao, Z. Gu, X. Xu, F. Zhang, Z. Lin, *Solid State Ionics* **2008**, *179*, 1697; b) H. Ye, Y. Li, *InfoMat* **2022**, *4*, e12291.
[9] a) D.-J. Lee, J.-W. Park, I. Hasa, Y.-K. Sun, B. Scrosati, J. Hassoun, *J. Mater. Chem. A* **2013**, *1*, 5256; b) N. Wang, Y. Wang, Z. Bai, Z. Fang, X. Zhang, Z. Xu, Y. Ding, X. Xu, Y. Du, S. Dou, G. Yu, *Energy Environ. Sci.* **2020**, *13*, 562; c) Y. Liang, B. Zhang, Y. Shi, R. Jiang, H. Zhang, *Materials* **2023**, *16*, 4263.
[10] M. Wild, L. O'Neill, T. Zhang, R. Purkayastha, G. Minton, M. Marinescu, G. J. Offer, *Energy Environ. Sci.* **2015**, *8*, 3477.
[11] a) W.-J. Li, C. Han, W. Wang, F. Gebert, S.-L. Chou, H.-K. Liu, X. Zhang, S.-X. Dou, *Adv. Energy Mater.* **2017**, *7*, 1700274; b) Q. Zhang, F. Li, J.-Q. Huang, H. Li, *Adv. Funct. Mater.* **2018**, *28*, 1804589; c) Y.-W. Song, L. Shen, N. Yao, X.-Y. Li, C.-X. Bi, Z. Li, M.-Y. Zhou, X.-Q. Zhang, X. Chen, B.-Q. Li, J.-Q. Huang, Q. Zhang, *Chem* **2022**, *8*, 3031.
[12] a) S. Xin, Y.-X. Yin, Y.-G. Guo, L.-J. Wan, *Adv. Mater.* **2014**, *26*, 1261; b) A. Manthiram, Y. Fu, S.-H. Chung, C. Zu, Y.-S. Su, *Chem. Rev.* **2014**, *114*, 11751.
[13] Z. Shadike, S. Tan, Q.-C. Wang, R. Lin, E. Hu, D. Qu, X.-Q. Yang, *Mater. Horiz.* **2021**, *8*, 471.
[14] H. Lyu, X.-G. Sun, S. Dai, *Adv. Energy Sustain. Res.* **2021**, *2*, 2000044.
[15] J. F. Mike, J. L. Lutkenhaus, *J. Polym. Sci., Part B: Polym. Phys.* **2013**, *51*, 468.
[16] a) L. W. Shacklette, J. E. Toth, N. S. Murthy, R. H. Baughman, *J. Electrochem. Soc.* **1985**, *132*, 1529; b) M. Morita, K. Komaguchi, H. Tsutsumi, Y. Matsuda, *Electrochim. Acta* **1992**, *37*, 1093.
[17] a) J. Tang, L. Kong, J. Zhang, L. Zhan, H. Zhan, Y. Zhou, C. Zhan, *React. Funct. Polym.* **2008**, *68*, 1408; b) B. Rasch, W. Vielstich, *J. Electroanal. Chem.* **1994**, *370*, 109.
[18] S. R. Sivakkumar, P. C. Howlett, B. Winther-Jensen, M. Forsyth, D. R. Macfarlane, *Electrochim. Acta* **2009**, *54*, 6844.
[19] a) Q. Zhang, Q. Ma, R. Wang, Z. Liu, Y. Zhai, Y. Pang, Y. Tang, Q. Wang, K. Wu, H. Wu, Y. Zhang, L. Zhang, C. Zhang, L. Fu, S. Eliseeva, V. Kondratiev, Y. Wu, *Mater. Today* **2023**, *65*, 100; b) P. Sang, Q. Chen, D.-Y. Wang, W. Guo, Y. Fu, *Chem. Rev.* **2023**, *123*, 1262.
[20] a) H. Kang, H. Kim, M. J. Park, *Adv. Energy Mater.* **2018**, *8*, 1802423; b) X. Li, L. Yuan, D. Liu, Z. Li, J. Chen, K. Yuan, J. Xiang, Y. Huang, *Energy Storage Mater.* **2020**, *26*, 570.
[21] J. Zhou, T. Qian, N. Xu, M. Wang, X. Ni, X. Liu, X. Shen, C. Yan, *Adv. Mater.* **2017**, *29*, 1701294.
[22] M. Wu, Y. Cui, A. Bhargav, Y. Losovyj, A. Siegel, M. Agarwal, Y. Ma, Y. Fu, *Angew. Chem., Int. Ed.* **2016**, *55*, 10027.
[23] S. Zeng, L. Li, J. Yu, N. Wang, S. Chen, *Electrochim. Acta* **2018**, *263*, 53.
[24] J. E. Bennett, H. Sieper, P. Tavs, *Tetrahedron* **1967**, *23*, 1697.
[25] H. Mutlu, P. Theato, *Macromol. Rapid Commun.* **2020**, *41*, 2000181.
[26] A. Takahashi, R. Goseki, H. Otsuka, *Angew. Chem., Int. Ed.* **2017**, *56*, 2016.
[27] a) J. Hobich, B. Huber, P. Theato, H. Mutlu, *Macromol. Rapid Commun.* **2021**, *42*, 2100118; b) H. Mutlu, D. A. Döpping, B. Huber, P. Theato, *Macromol. Rapid Commun.* **2021**, *42*, 2000695.
[28] S. S. Zhang, *J. Power Sources* **2013**, *231*, 153.
[29] a) X. Yang, X. Gao, Q. Sun, S. P. Jand, Y. Yu, Y. Zhao, X. Li, K. Adair, L.-Y. Kuo, J. Rohrer, J. Liang, X. Lin, M. N. Banis, Y. Hu, H. Zhang, X. Li, R. Li, H. Zhang, P. Kaghazchi, T.-K. Sham, X. Sun, *Adv. Mater.* **2019**, *31*, 1901220; b) Z. Wei Seh, W. Li, J. J. Cha, G. Zheng, Y. Yang, M. T. Mcdowell, P.-C. Hsu, Y. Cui, *Nat. Commun.* **2013**, *4*, 1331; c) X. Li, M. Banis, A. Lushington, X. Yang, Q. Sun, Y. Zhao, C. Liu, Q. Li, B. Wang, W. Xiao, C. Wang, M. Li, J. Liang, R. Li, Y. Hu, L. Goncharova, H. Zhang, T.-K. Sham, X. Sun, *Nat. Commun.* **2018**, *9*, 4509.
[30] a) G. G. Eshetu, G. A. Elia, M. Armand, M. Forsyth, S. Komaba, T. Rojo, S. Passerini, *Adv. Energy Mater.* **2020**, *10*, 2000093; b) X. Xu, D. Zhou, X. Qin, K. Lin, F. Kang, B. Li, D. Shanmukaraj, T. Rojo, M. Armand, G. Wang, *Nat. Commun.* **2018**, *9*, 3870.
[31] L. Lodovico, A. Varzi, S. Passerini, *J. Electrochem. Soc.* **2017**, *164*, A1812.
[32] Y. Li, K. K.. Fu, C. Chen, W. Luo, T. Gao, S. Xu, J. Dai, G. Pastel, Y. Wang, B. Liu, J. Song, Y. Chen, C. Yang, L. Hu, *ACS Nano* **2017**, *11*, 4801.
[33] a) H. Ding, Z. Pan, L. Pigani, R. Seeber, C. Zanardi, *Electrochim. Acta* **2001**, *46*, 2721; b) J. Heinze, B. A. Frontana-Uribe, S. Ludwigs, *Chem. Rev.* **2010**, *110*, 4724.
[34] a) L. Liu, F. Tian, X. Wang, Z. Yang, M. Zhou, X. Wang, *React. Funct. Polym.* **2012**, *72*, 45; b) L. M. Zhu, A. W. Lei, Y. L. Cao, X. P. Ai, H. X. Yang, *Chem. Commun.* **2013**, *49*, 567.
[35] G. A. Muller, J. B. Cook, H.-S. Kim, S. H. Tolbert, B. Dunn, *Nano Lett.* **2015**, *15*, 1911.
[36] a) G. P. López, D. G. Castner, B. D. Ratner, *Surf. Interface Anal.* **1991**, *17*, 267; b) K. L. Parry, A. G. Shard, R. D. Short, R. G. White, J. D. Whittle, A. Wright, *Surf. Interface Anal.* **2006**, *38*, 1497; c) S. Komaba, W. Murata, T. Ishikawa, N. Yabuuchi, T. Ozeki, T. Nakayama, A. Ogata, K. Gotoh, K. Fujiwara, *Adv. Funct. Mater.* **2011**, *21*, 3859; d) T. Sultana, G. L. Georgiev, G. Auner, G. Newaz, H. J. Herfurth, R. Patwa, *Appl. Surf. Sci.* **2008**, *255*, 2569.
[37] Z. Zeng, W. Li, Q. Wang, X. Liu, *Adv. Sci.* **2019**, *6*, 1900711.
[38] M. Helen, M. A. Reddy, T. Diemant, U. Golla-Schindler, R. J. Behm, U. Kaiser, M. Fichtner, *Sci. Rep.* **2015**, *5*, 12146.
[39] V. Nilsson, A. Kotronia, M. Lacey, K. Edström, P. Johansson, *ACS Appl. Energy Mater.* **2020**, *3*, 200.